Electronic Supplementary Information

Exploring Porosity in a Flexible 3D Organic-Inorganic {Zn$^{II}_3$(4DPNDI)[W^V(CN)$_8$]$_2$} Coordination Network

Katarzyna Jędrzejowska[1,2], Jedrzej Kobylarczyk[3], Tadeusz M. Muzioł[4], Beata Nowicka[1], Damian Jędrzejowski[1,2], Dariusz Matoga[1], Bartłomiej Gaweł,[5] Robert Podgajny[1]*

[1] *Faculty of Chemistry, Jagiellonian University in Krakow, Gronostajowa 2, 30-387 Kraków, Poland; katarzyna.jedrzejowska@doctoral.uj.edu.pl (K.J); beata.nowicka@uj.edu.pl (B.N); damian.jedrzejowska@doctoral.uj.edu.pl (D.J); dariusz.matoga@uj.edu.pl (D.M.); robert.podgajny@uj.edu.pl (R.P.)*

[2] *Doctoral School of Exact and Natural Sciences, Jagiellonian University in Kraków, Prof. St. Łojasiewicza 11, 30-348 Kraków, Poland; katarzyna.jedrzejowska@doctoral.uj.edu.pl (K.J.) damian.jedrzejowska@doctoral.uj.edu.pl (D.J)*

[3] *Institute of Nuclear Physics PAN, Radzikowskiego 152, 31-342 Kraków, Poland; jedrzej.kobylarczyk@ifj.edu.pl (J.K.)*

[4] *Faculty of Chemistry, Nicolaus Copernicus University in Toruń, Gagarina 7, 87-100 Toruń, Poland; tmuziol@umk.pl (T.M.M.)*

[5] *The Quartz Corp, Hellandsveien 14, 8270 Drag, Norway, bartlomiej.gawel@thequartzcorp.com (B.G)*

* *Correspondence: robert.podgajny@uj.edu.pl (R.P.). Tel. +48-12-686-2459 (R.P.)*

Spis treści

1. Details of structural description

Table S1. Crystal data and structure refinement of **1**, and **2·DMA**.

| Compound		**1**	**2·DMA**
Crystal data			
formula		$C_{24}H_{36}N_{12}O_4Zn_{1.5}W$	$C_{80}H_{102}N_{30}O_{14}Zn_3W_2$
formula weight / g·mol^{-1}		838.55	2271.72
T / K		100.0	100.0
λ / Å		0.71073 (MoKα)	
crystal system		Triclinic	
space group		*P*-1	
cell parameters	*a* / Å	9.8046(7)	9.7937(4)
	b / Å	11.0611(7)	16.0738(7)
	c / Å	16.2733(11)	19.6573(9)
	α / deg	85.355(3)	103.573(2)
	β / deg	83.387(4)	102.206(2)
	γ / deg	68.662(3)	94.0730(10)
	V / Å^3	1631.46(19)	2916.3(2)
Z		2	1
ρ_{calc} / g·cm^{-3}		1.707	1.294
μ / cm^{-1}		4.665	2.634
F(000)		830.0	1142.0
crystal type		yellow block	orange block
crystal size / mm × mm × mm		0.6 × 0.2 × 0.2	0.34 × 0.19 × 0.11
Data collection			
2θ range / deg		3.956 to 51.39	5.06 to 50.052
limiting indices		-11 ⩽ h ⩽ 9 -13 ⩽ k ⩽ 13 -19 ⩽ l ⩽ 19	-10 ⩽ h ⩽ 11 -19 ⩽ k ⩽ 19 -23 ⩽ l ⩽ 23
collected reflections		18045	21255
independent reflections		6083 [R_{sigma} = 0.0620]	10077 [R_{sigma} = 0.0616]
R_{int}		0.0528	0.0350
Refinement			
data/restraints/parameters		6083/8/397	10077/59/541
GOF on *F^2*		1.163	1.095
final *R* indices		R_1 = 0.0488 [I ⩾2σ(I)] wR_2 = 0.1079 (all data)	R_1 = 0.0506 [I ⩾2σ(I)] wR_2 = 0.1226 (all data)
largest diff. peak/hole / e·Å^{-3}		3.10/-2.17	3.04/-2.01
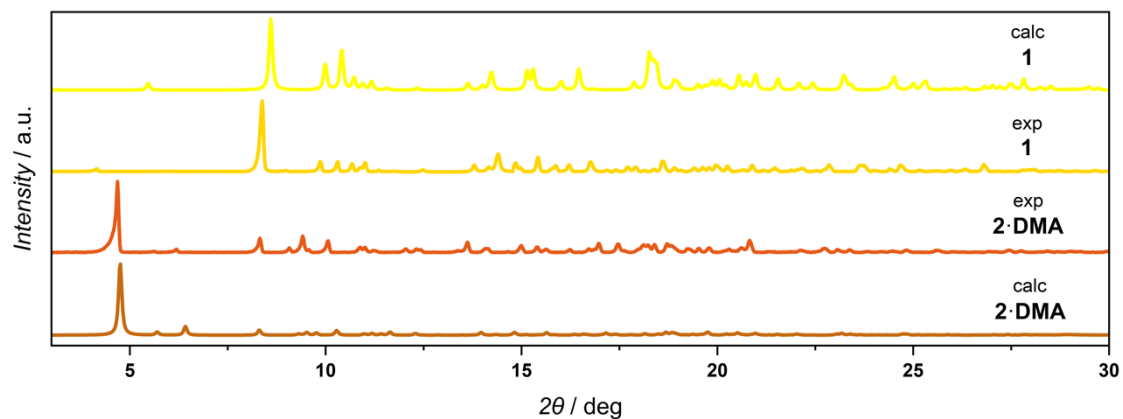
Figure S1. Experimental room-temperature PXRD patterns of the polycrystalline samples of **1** and **2·DMA** in mother solution (RT, exp), compared with the PXRD patterns simulated based on the respective SC XRD data (T = 100 K, calc).
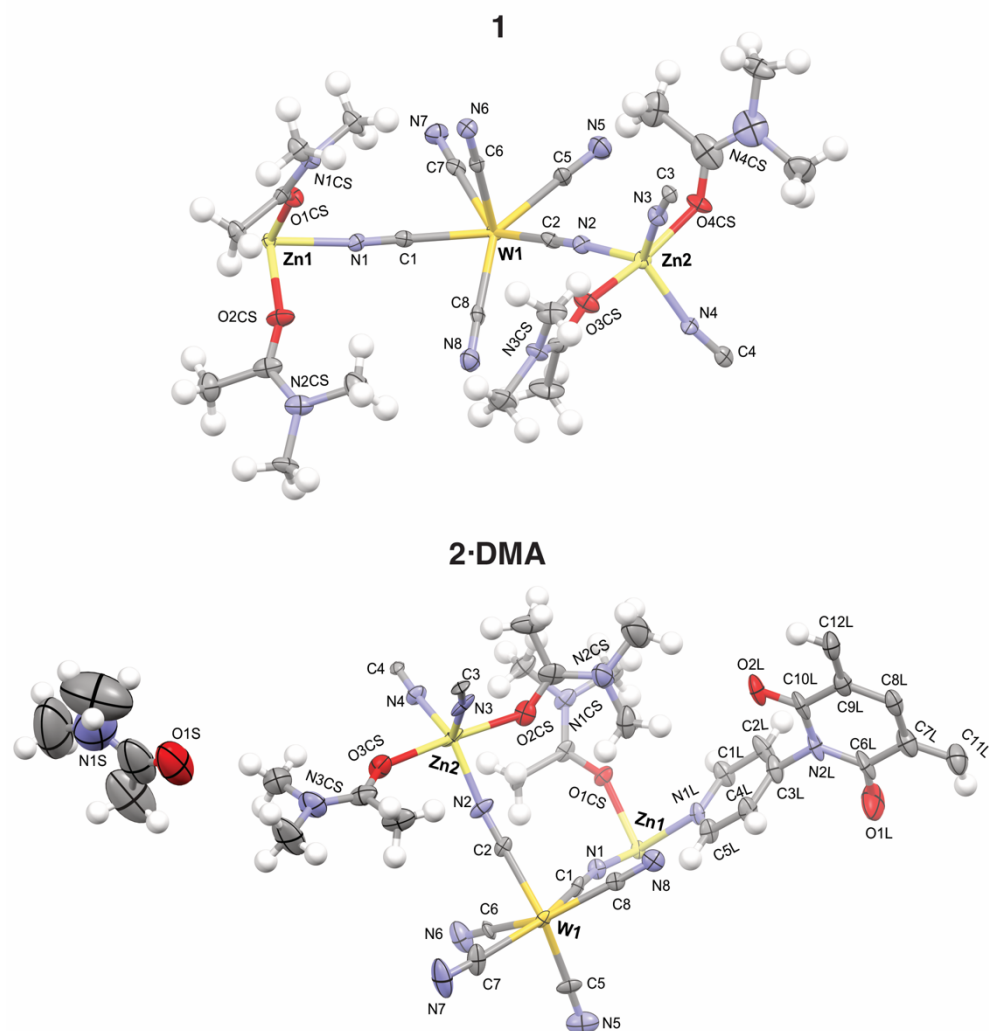

Figure S2. Asymmetric units of **1** and **2·DMA**. Colors: gold – W, light yellow – Zn, grey – C, blue – N, red – O, white– H. The thermal ellipsoids are drawn at the 50% probability level.

The inorganic layers of both compounds comprise $[W^V(CN)_8]^{3-}$ and Zn^{2+} ions. The eight-coordinated $[W^V(CN)_8]^{3-}$ moiety adopts slightly distorted square antiprism geometry in **1**, whereas in **2·DMA** it exhibits a slightly distorted triangular dodecahedron geometry, both typical for octacyanotungstates. Each $[W(CN)_8]^{3-}$ forms three bridges to the neighboring Zn^{II} ions, while the remaining five cyanide groups remain terminal. The W1–C bond lengths range from 2.146(9) to 2.180(8) Å in compound **1** and from 2.137(7) to 2.188(8) Å in compound **2·DMA**. Additionally, the W1–C–N angles exhibit nearly linear geometry, deviating from linearity by a maximum of 3.4 and 4.6 degrees in compounds **1** and **2·DMA**, respectively.

Each compound contains two crystallographically independent Zn(II) centers, denoted as Zn1 and Zn2. Zn1 moieties are six-coordinated, forming either an octahedral $\{Zn^{II}N_2O_4\}$ environment in compound **1** or an octahedral $\{Zn^{II}N_4O_2\}$ environment in compound **2·DMA**. In compound **1**, Zn1 is surrounded by two cyano-nitrogen atoms alligned in *trans*-geometry and four oxygen atoms from DMA molecules, with bond lengths Zn1–N1, Zn1–O1CS, and Zn1–O2CS measured at 2.105(7), 2.110(6), and 2.103(6) Å, respectively. In contrast, in compound **2·DMA**, each Zn1 atom is surrounded by two cyano-nitrogen atoms, two pyridine nitrogen atoms from DPNDI ligands, and two oxygen atoms from DMA molecules, all three pairs of ligands alligned in *trans*-geometry, with bond lengths Zn1–N1, Zn1–NL1, and Zn1–O1CS measured at 2.158(5), 2.120(5), and 2.123(5) Å, respectively.

Zn2 moieties in both structures are coordinated by five atoms, forming a trigonal bipyramidal $\{Zn^{II}N_3O_2\}$ environment composed of three N atoms of cyanido-bridges located in equatorial plane and two O atoms of DMA in the axial direction. In compound **1**, the bond lengths for Zn2–N2, Zn2–N3, and Zn2–N4 are measured at 1.987(7), 2.011(8), and 1.983(7) Å, respectively, while in compound **2·DMA**, these bond lengths are measured at 2.007(6), 2.031(6), and 2.000(5) Å, respectively. Additionally, the bond lengths for Zn2–O3CS and Zn2–O4CS are 2.087(6) and 2.098(6) Å in compound **1**, and 2.112(5) (Zn2–O2CS) and 2.076(5) (Zn2–O3CS) Å in compound **2·DMA**. Furthermore, the Zn1–N–C and Zn2–N–C bonds in both structures exhibit different degree of bending, ranging from 166.7 to 174.4 degrees in compound **1** and from 167.8 to 175.1 egrees in compound **2·DMA**. This is correlated with more distorted trigonal bipyramidal environment for **2·DMA** compared to **1**.

As for the formula of **2·DMA**, $\{Zn^{II}_3(DMA)_6[W^V(CN)_8]_2(4DPNDI)\cdot 8DMA\}$, derived from the SCXRD analysis and DVS measuremetns, three types of DMA molecules are distinguished in the achieved crystallographic model. Per one Zn_3W_2DPNDI unit we have found six coordinated molecules, whereas among eight crystallization DMA molecules two molecules are detected in a close intermolecular contact with the surfaces of one 4DPNDI core. The remainig six DMA molecules per Zn_3W_2DPNDI unit are disordered within the porous space, modelled using the SQUEEZE procedure.

Table S2. The most important bond lengths (in Å) and angles (in deg) for **1**, and **2·DMA**. Detailed metric parameters of octacyanotungstates anion.

compound	**1**	**2·DMA**
	2.168(8)	2.168(6)
	2.146(9)	2.152(7)
	2.157(8)	2.164(6)
W1–C	2.168(9)	2.158(6)
	2.150(8)	2.137(7)
	2.180(8)	2.162(6)
	2.173(8)	2.188(8)
	2.148(8)	2.158(7)
	1.139(10)	1.141(8)
	1.138(11)	1.136(8)
	1.145(11)	1.140(8)
C≡N	1.153(10)	1.138(8)
	1.147(11)	1.154(9)
	1.138(10)	1.149(9)
	1.150(10)	1.116(10)
	1.170(10)	1.150(8)
	179.1(7)	177.6(5)
	178.3(7)	178.2(5)
	176.6(7)	176.7(6)
W1–C≡N	176.6(7)	179.4(6)
	177.8(8)	179.2(8)
	178.3(7)	177.3(7)
	177.6(7)	175.4(8)
	178.6(7)	178.1(6)

Table S3. The most important bond lengths (in Å) and angles (in deg) for **1**, and **2·DMA**. Detailed metric parameters of zinc(II) ions.[a]

compound	1	2·DMA
Zn1–N1	2.105(7)	2.158(5)
Zn1–NL1	-	2.120(5)
Zn1–O1CS	2.110(6)	2.123(5)
Zn1–O2CS	2.103(6)	-
Zn1–N1≡C1	174.4(6)	169.5(5)
Zn1–NL1	-	180.0
Zn1–O1CS–C1CS	140.9(5)	139.7(4)
Zn1–O2CS–C5CS	147.6(7)	-
Zn2–N2	1.987(7)	2.007(6)
Zn2–N3	2.011(8)	2.031(6)
Zn2–N4	1.983(7)	2.000(5)
Zn2–O2CS	-	2.112(5)
Zn2–O3CS	2.087(6)	2.076(5)
Zn2–O4CS	2.098(6)	-
Zn2–N2≡C2	171.2(7)	167.8(6)
Zn2–N3≡C3	174.3(7)	169.0(6)
Zn2–N4≡C4	166.7(6)	175.1(6)
Zn2–O3CS– C9CS	149.1(6)	135.2(5)
Zn2–O4CS– C13CS	127.5(6)	-

[a] NX – cyano-nitrogen atom from the $[W(CN)_8]^{3-}$ anions; NL1 – nitrogen atom from the DPNDI ligannds; OXCS – oxygen atom from the DMA molecules, where X = 1, 2, 3.

Table S4. Results of Continuos Shape Measure Analysis for $[W(CN)_8]^{3-}$ – **W1**, $[Zn(DMA)_4(NC)_2]$ (**1**) or $[Zn(DMA)_2(\mu\text{-}4DPNDI)_2(\mu\text{-}NC)_2]$ (**2·DMA**) – **Zn1**, and $[Zn(DMA)_2(NC)_3]^-$ – **Zn2**.

Atom	Compound	CSM parameters*			Geometry
		SAPR-8	**TDD-8**	**BTPR-8**	
W1	**1**	0.392	1.696	1.440	**SAPR-8**
	2·DMA	2.368	0.318	1.755	**TDD-8**
		PPY-6	**OC-6**	**TPR-6**	
Zn1	**1**	29.555	0.094	16.071	**OC-6**
	2·DMA	29.161	0.180	15.943	**OC-6**
		TBPY-5	**SPY-5**	**JTBPY-5**	
Zn2	**1**	0.861	3.324	2.970	**TBPY-5**
	2·DMA	0.326	3.668	2.604	**TBPY-5**

* CSM parameters:

CSM SAPR-8 = the parameter related to the square antiprism (D_{4d} symmetry)

CSM TDD-8 = the parameter related to the triangular dodecahedron (D_{2d} symmetry)

CSM BTPR-8 = the parameter related to the biaugmented trigonal prism (C_{2v} symmetry)

CSM PPY-6 = the parameter related to the pentagonal pyramid (C_{5v} symmetry)

CSM OC-6 = the parameter related to the octahedron (O_h symmetry)

CSM TPR-6 = the parameter related to the trigonal prism (D_{3h} symmetry)

CSM TBPY-5 = the parameter related to the trigonal bipyramid (D_{3h} symmetry)

CSM SPY-5 = the parameter related to the square pyramid (C_{4v} symmetry)

CSM JTBPY-5 = the parameter related to the Johnson trigonal bipyramid (D_{3h} symmetry)

CSM = 0 for the ideal geometry and the increase of CSM parameter corresponds to the increasing distortion from the ideal polyhedron.

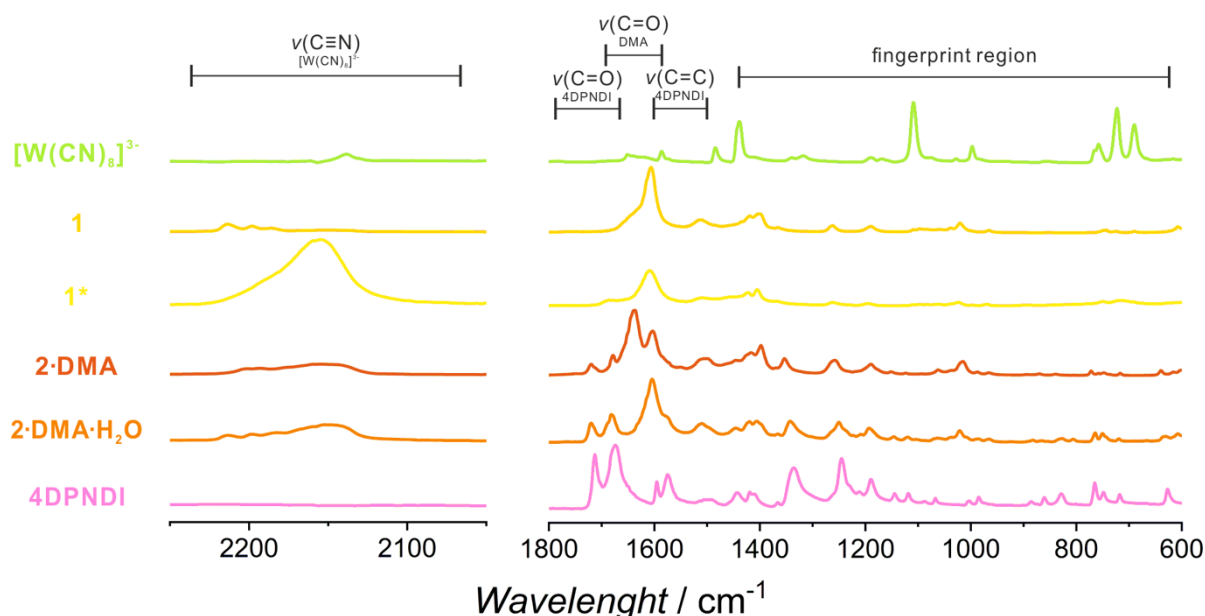## 2. Details of spectroscopic characterization

2.1. Vibrational studies

Figure S3. Infrared spectra were collected at room temperature for polycrystalline samples of $(PPh_4)_3[W(CN)_8]\cdot 3H_2O$ and 4DPNDI, as well as for **1** and **2·DMA** (in mother liquor), and their corresponding dried forms, **1*** and **2·DMA·H₂O**.

The IR spectra reveal distinct bands corresponding to molecular components and intermolecular interactions, as elucidated by SC XRD analysis. These bands encompass the $\nu(C\equiv N)$ vibration around 2155 cm^{-1} for $[W(CN)_8]^{3-}$ and a series of backbone vibrations for 4DPNDI and PPh_4^+ (refer to Figure S3). Specifically, the infrared-active $\nu(C\equiv N)$ vibrations exhibit shifts of: 2214, 2198 cm^{-1} for **1**; 2155 cm^{-1} for **1***; 2202, 2195, and 2153 cm^{-1} for **2·DMA**; 2214, 2198, 2152 cm^{-1} for **2·DMA·H₂O**. These shifts typically range between 20-80 cm^{-1} higher in wavelength compared to the corresponding precursor $(PPh_4)_3[W(CN)_8]$. Concerning the skeletal linker IR-active vibrations, notable spectral shifts of approximately 10 cm^{-1} (for the 4DPNDI line) are observable in the region of 1720-1670 cm^{-1}, which corresponds to the $\nu(C=O)$ type vibrations. These shifts can be distinguished from the contributions of other components. All observed alterations compared to the reference solids stem from the bonding network within the inorganic layers of materials **1**, **1***, **2·DMA** and **2·DMA·H₂O**, as well as the coordination bonds in **2·DMA** formed between the inorganic layers and the linker represented by 4DPNDI. In particular, the changes in the solvent space occupation might be decisive in

significant modifications of $\nu(C\equiv N)$ vibration patterns, due to the change in non-covalent interactions (e.g. hydrogen bonds) involving nitrogen atoms (Figure S3). The $\nu(C=O)$ vibrations are diagnostic for the number of DMA molecules, which is best illustrated in the variable intensity of the peak close to 1650 cm^{-1} observed in the native specimen of **2·DMA**, the specimen **2·DMA·H$_2$O** obtained after partial exchange of DMA with atmospheric H$_2$O, and the specimen **2·DMA** regenerated in DMA (Figure S4).
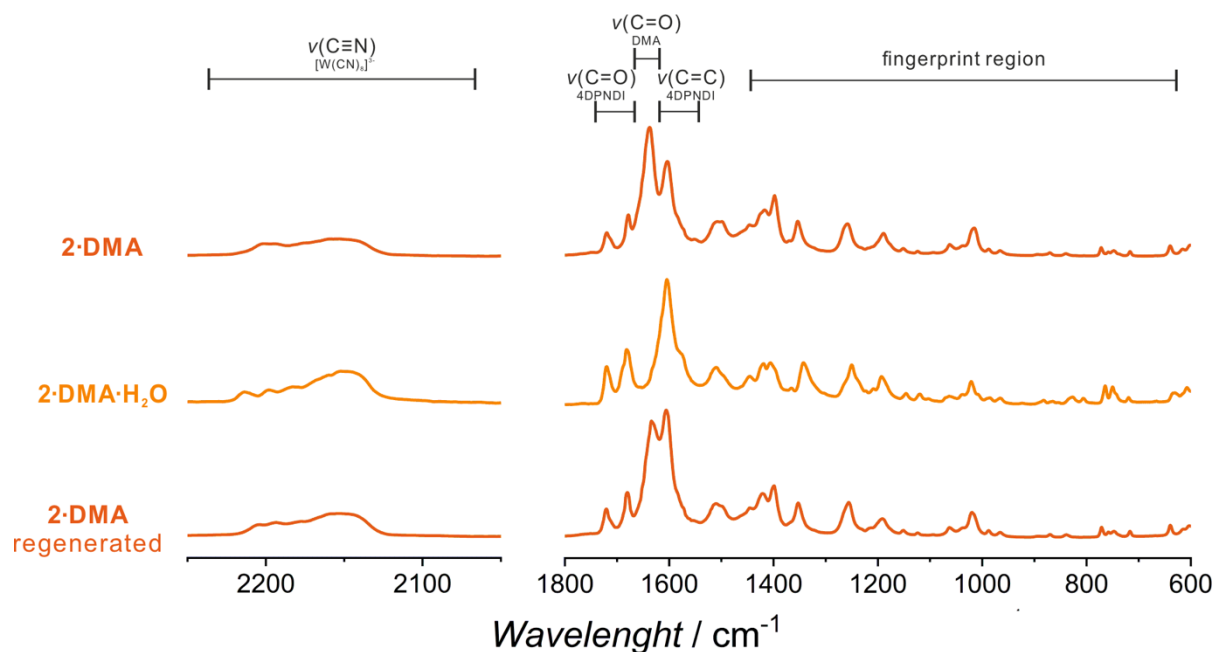

Figure S4. Infrared spectra were obtained at room temperature for polycrystalline samples of **2·DMA** (in mother liquor), **2·DMA·H$_2$O**, and **2·DMA** regenerated in pure DMA following the regeneration process.

2.2. Sorption studies

2.2.1. Dynamic vapour sorption

Dynamic vapour sorption studies using gravimetric technique were performed under changable partial pressure of different solvents vapours in the flow of N_2. In order to avoid exposure to air moisture, freshly prepared samples of **2·DMA** were washed by decantation with DMA, filtered off, and placed immediately under dry nitrogen flow in the DVS apparatus chamber at 25 °C, without air-drying. The initial fast mass loss connected with the evaporation of surface DMA, which lasted about 20 minutes, was followed by two desolvation steps with slower mass loss rate, which lasted about 1 and 5 days, respectively. The mass loss in these steps corresponds to the release of about 5 (step 1) and 3 (step 2) DMA molecules, 8 DMA molecules in total. This amount is consistent with the total solvent accesible volume in the structure of **2·DMA** of 1265 Å per formula unit and molecular volume of liquid DMA of 158 Å. Considering the amount of mass loss and lack of changes in the PXRD pattern (Figure 2), we conclude that after desolatation phase **2** is obtained, which cointains the original 6 molecules of coordinated DMA, but no lattice DMA, producing the $\{Zn^{II}_3(DMA)_6[W^V(CN)_8]_2(4DPNDI)\}$ formula. The resulting phase **2** was then studied by H_2O or MeOH sorption. The mass registered upon stepwise changes in relative humidity (RH) in the first sorption cycle (Figure S5a left), in addition to typical increase connected to the intake of H_2O, shows anomalous decrease upon reaching certain RH values (22, 50, and 92 %RH), which can be attributed to the exchange of coordinated DMA by lighter H_2O molecules. After full sorption-desorption cycle the sample mass decreases by 21.5 %, which is consistent with the exchange of all 6 coordinated DMA molecules by water. Similar behaviour is observed upon MeOH sorption with anomalous mass loss at 30% p/p_0 (Figure S5b left). Second sorption cycles show characteristics of a microporous material, with sharp initial vapour intake and relatively narrow hysteresis (Figure S6). The increase in mass of about 16% (H_2O) and 14.5% (MeOH) corresponds to the intake of additional 13.5 H_2O molecules or 7 MeOH, which is much less than the the potential capacity of the original voids in the structure of **2·DMA**. This indicates that the exchange of coordinated DMA causes significant deformation of the structure with closing of the pores and formation of a new phase denoted as **2·H$_2$O**. This supposition is corroborated by the PXRD patterns recorded for samples exposed to high humidity (Figure 2). Subsequent sorption cycles show decrease in the maximum water intake indicating further structural changes and gradual degradation confirmed by PXRD. Experiments with the sorption of other volatile solvents (Figure S6) show moderate

(CHCl$_3$) or negligible sorption (hexane, toluene), which is most probably connected with their larger size and lower polarity.
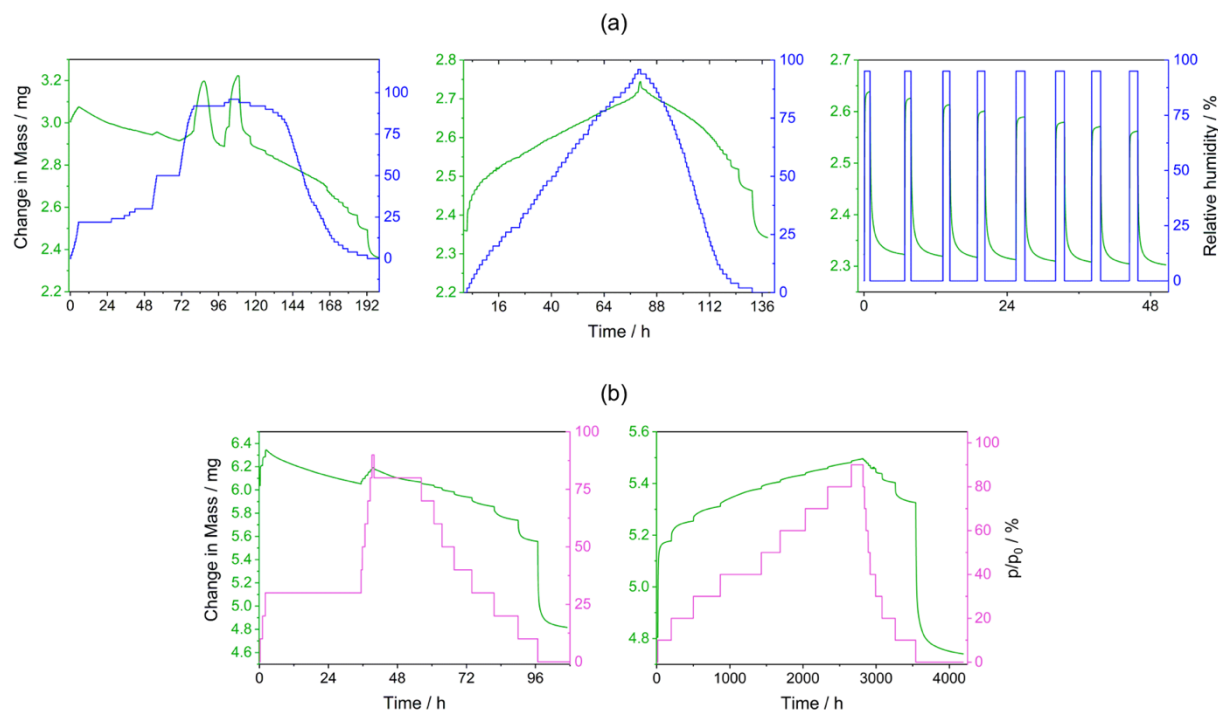

Figure S5. Changes in mass and p/p$_0$ registered in water (a) and MeOH (b) sorption experiments
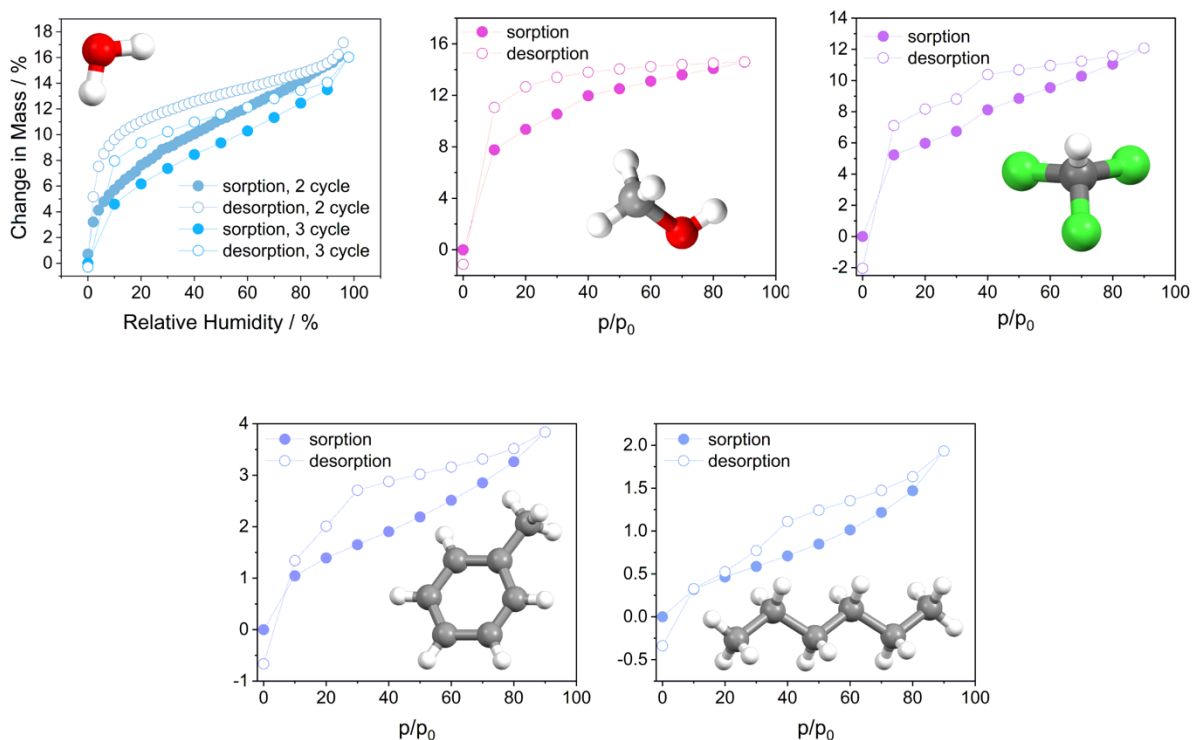

Figure S6. Water, methanol, chloroform, toluene, and hexene vapor sorption isotherms at 295 K measured using a dynamic vapor sorption (DVS) method.
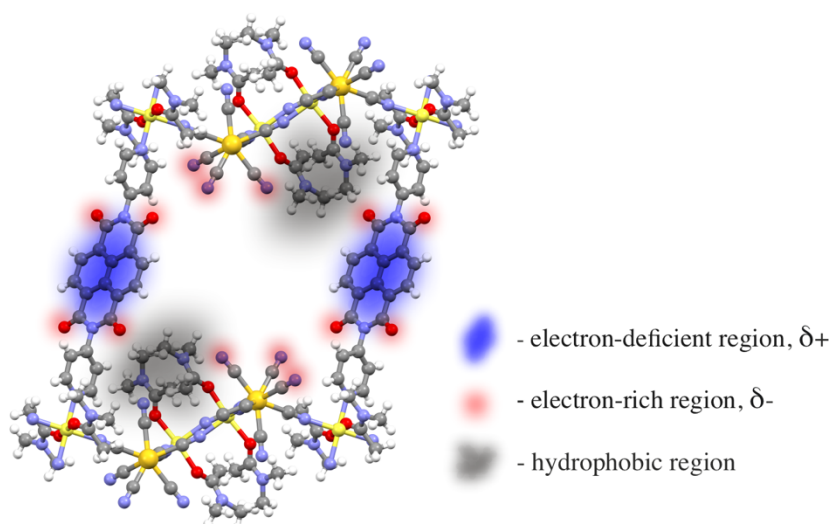
Figure S7. Cross-sectional view of the interior channel in a **2·DMA** with the different regions highlighted by colored spots: blue – electron-deficient areas (δ+), red – indicates electron-rich sites (δ-), gray – hydrophobic regions. Atoms: gold – W, light yellow – Zn, grey – C, blue – N, red – O, white– H.

2.2.2. ^{1}H NMR characterisation of 2* material

The **2*** material was obtained by vacuum activation (10^{-3} mbar) at 40 °C. Removal of guest molecules was expected under such conditions. To verify whether the DMA molecules coordinating to the zinc ions (6 molecules per Zn_3W_2 unit, according to crystal structure of **2·DMA**) are also removed or remain coordinated, additional analysis of the material was required.

Among the techniques that can enable compositional analysis, ^{1}H NMR spectroscopy was the only technique for determining DMA content in the case studied. Two different approaches involving samples digestion and standard addition were used for this purpose.

A   Considering the fact that the tungsten present in the compound is paramagnetic, in order to obtain a spectrum of good quality after the material was digested, an inorganic fraction was separated from the organic fraction. For this purpose, 44.2 mg of **2*** was digested by adding approximately 0.5 mL of H_2SO_4 and approximately 4 ml of water. The resulting light yellow solution with a white precipitate was extracted with three 1.5 mL portions of $CDCl_3$. To the combined organic solutions, 21.9 mg of dicyanobenzene was added as a standard and 800 μL of such prepared solution was taken for measurement.

B   In the second approach, direct **2*** digestion was used, and two samples (**B1**, and **B2**) were prepared for better approximation. For this purpose, 25.8 and 16.9 mg of the **2*** material were weighed, 100 μL of D_2SO_4 and 1.0 mL of DMSO-d_6 were added to each vial and sonicated for 1-2 min. Then 9.3 and 7.2 mg of terephthalic acid were added, respectively. The digestion resulted in a clear yellow solution, 750 μL of which was taken for measurement.
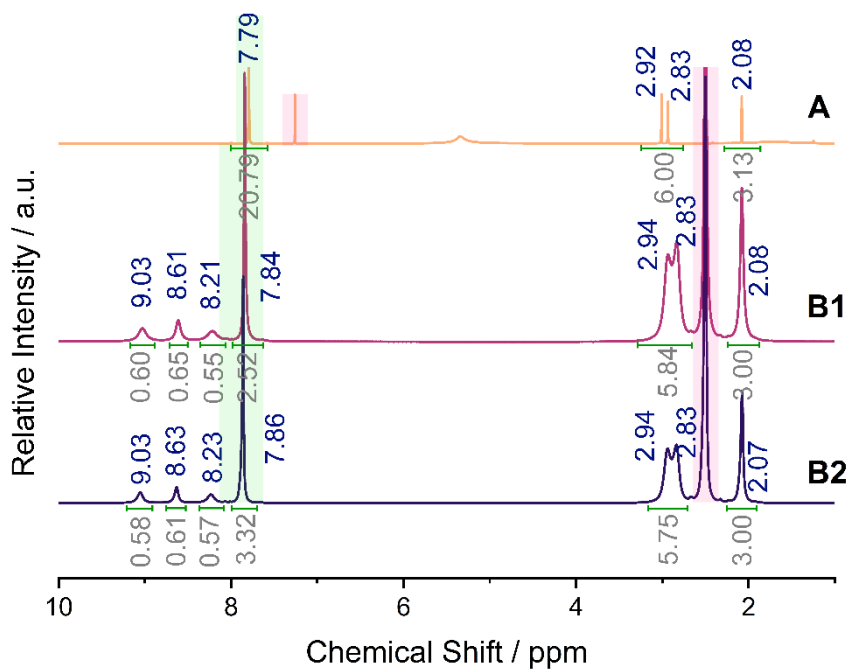
Figure S8. ^{1}H NMR spectra for the solutions obtained through the digestion of **2***. The spectra were prepared in three variants: **A**, **B1**, and **B2** (described in more detail above). Signals from the solvent are highlighted in pink: **A** – CDCl$_3$; **B1** and **B2** – DMSO-d$_6$. Signals from standards are highlighted in green: **A** – dicyanobenzene; **B1**, **B2** – terephthalic acid.

Procedure **A** provided a **lower estimate** of the number of DMA molecules. In this case, only DMA was eluted into the organic phase (CDCl$_3$). The DPNDI ligand and inorganic fragments remained in the aqueous phase or undissolved. The signals at 2.08, 2.83 and 2.92 ppm (spectrum **A**) originate from the three methyl groups of the DMA molecule. The signal from the standard (dicyanobenzene) is located at 7.79 ppm. By averaging the integration of the DMA signals and dividing by the number of protons, the molar ratio of dicyanobenzene:DMA can be determined to be equal to about 5.04. Assuming that the dissolved material contained only the Zn$_3$W$_2$(DPNDI) backbone and 6 coordinating DMA molecules, its molar mass is equal to 1923.2 g/mol. Considering the mass of the dissolved material and the mass of the standard, the number of DMA molecules in the skeleton can thus be calculated to be equal to about **1.5 per unit of Zn$_3$W$_2$**. It should be noted that this result is twice *underestimated*: First, the **2*** material at the time of weighing certainly contained water molecules in the pores, so its molar mass was higher. Second, DMA is soluble in both water and CDCl$_3$, so only a portion of it was extracted. The value obtained should therefore be considered an underestimate.

Procedure **B** provided a closer estimation of the number of DMA molecules. The first approximation of DMA content was based on the ratio of the average signal from DMA

molecules (2.08, 2.83 and 2.94 ppm) and the average signal from DPNDI (8.21, 8.61 and 9.03 ppm) molecules. This estimation was possible due to the fact that in this case all the material had undergone digestion. A DMA:DPNDI ratio of **6.55** was obtained for the first sample (spectrum **B1**), and **6.61** for the second (spectrum **B2**). The second estimate of DMA content was based on a comparison of DMA signals integration and the standard (terephthalic acid, 7.86 ppm) integration. In order to calculate the number of DMA molecules, the molar mass of the weighed **2*** material was assumed to be between 1923 (Zn_3W_2(DPNDI) skeleton + 6 DMA molecules) and 2103 g/mol (as above + 10 additional water molecules in the pores). For the first sample (**B1**), this resulted in a DMA content of **6.50-7.11** molecules per Zn_3W_2 unit, while for the second sample (**B2**) it resulted in **5.77-6.32** molecules.

Averaging the results from the first approximation and the lower bounds (as more probable) from the second approximation, taking into account the uncertainty as the standard deviation, the average DMA content of skeleton **2*** is obtained as equal to **6.4±0.3** per Zn_3W_2 unit. Including statistical errors, weighting error, and error in reading integration from the spectra, the DMA content should be considered equal to 6 molecules per Zn_3W_2 unit and possibly an additional small fraction of a molecule in the pores (although the latter is subject to large uncertainties).

*2.2.3. PXRD characterization of **2*** material*

The sample of **2*** for PXRD measurements was prepared under the inert atmosphere to avoid the changes that might be expected under contact with humidity in ambient conditions. The powder diffractogram for **2*** is presented in Figure S9 (yellow line). The best indexing attempt illustrated by the dark blue line in Figure S9 led to the triclinic cell with a parameters set: $a =$ 16.528 Å, $b =$ 16.16649 Å, $c =$ 20.399 Å, $\alpha =$ 128.165°, $\beta =$ 108.458°, $\gamma =$ 91.642°, $V =$ 3876.91 Å^3. The positions of diffraction peaks in the measured diffractogram and in the calculated one are in satisfactory agreement. Some cell parameters differ notably from those found for **2·DMA**, triclinic cell $a =$ 9.7937 Å, $b =$ 16.0738 Å, $c =$ 19.6573 Å, $\alpha =$ 103.573°, $\beta =$ 102.206°, $\gamma =$ 94.0730°, $V =$ 2916.3 Å^3. However, we found that the general orientation of a, b and γ parameters of the new cell, considered as oriented parallel to the Zn_3W_2 layers, might be maintained to reasonably describe their 2D arrangement. This assumption is strongly supported by the inherent non-rigidity of cyanido-bridged skeletons widely observed in the literature[1–3] due to the broad spectrum of M(3d metal ion)-N-C angles (see also the structural data for independetly grown crystals of **2·DMA** and **1**, above), in broadest context between 180 and 140 deg. Furthermore, the value of the α angle increased from 103.573° for **2·DMA** to 128.165° for **2*** suggesting a significant tilt of the DPNDI ligand in respect to the Zn_3W_2 in **2*** compared to **2·DMA.** This is consistent with the assumption that after the removal of crystallization solvent molecules, the coordination network undergoes some closure and a reduction of porous space, as was suggested by PXRD studies of the phases undergoing solvent sorption (see Figure 2 in the main text) and by the N_2 and CO_2 sorption studies of **2*** (see below). The increase in the length of the c period, going from **2·DMA** to **2***, is rather minor, which reasonably supports the general description of the observed structural transition **2·DMA → 2***, and provides the overall image of the possible pathways of other structural changes accompanying the studies sorption processes.
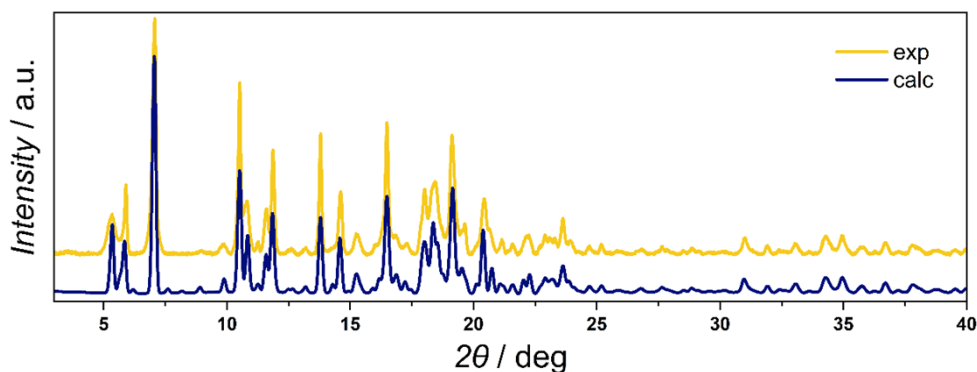

Figure S9. Experimental room-temperature PXRD pattern of the polycrystalline samples of **2*** under an inert gas (RT, exp), compared with the simulated PXRD pattern (RT, calc).

Notingly, the experimental powder diffractogram of **2*** (yellow line in Figure S9) reveals a broadening of some peaks, for example nicely represented by the first peak located just above the $2\theta = 5°$. This broadening may be attributed to the presence of crystallites with varying orientation of the DPNDI and DMA ligands (due to rotational freedom) or/and, more importantly, to the degree of structural closure within a polycrystalline sample, leading to a non-discrete distribution of interlayer distances with variable tilting angles of the DPNDI ligands. Nevertheless, skeleton is likely to be preserved. Full structure determination was, however, not possible due to complexity of the structure and peaks broadening.
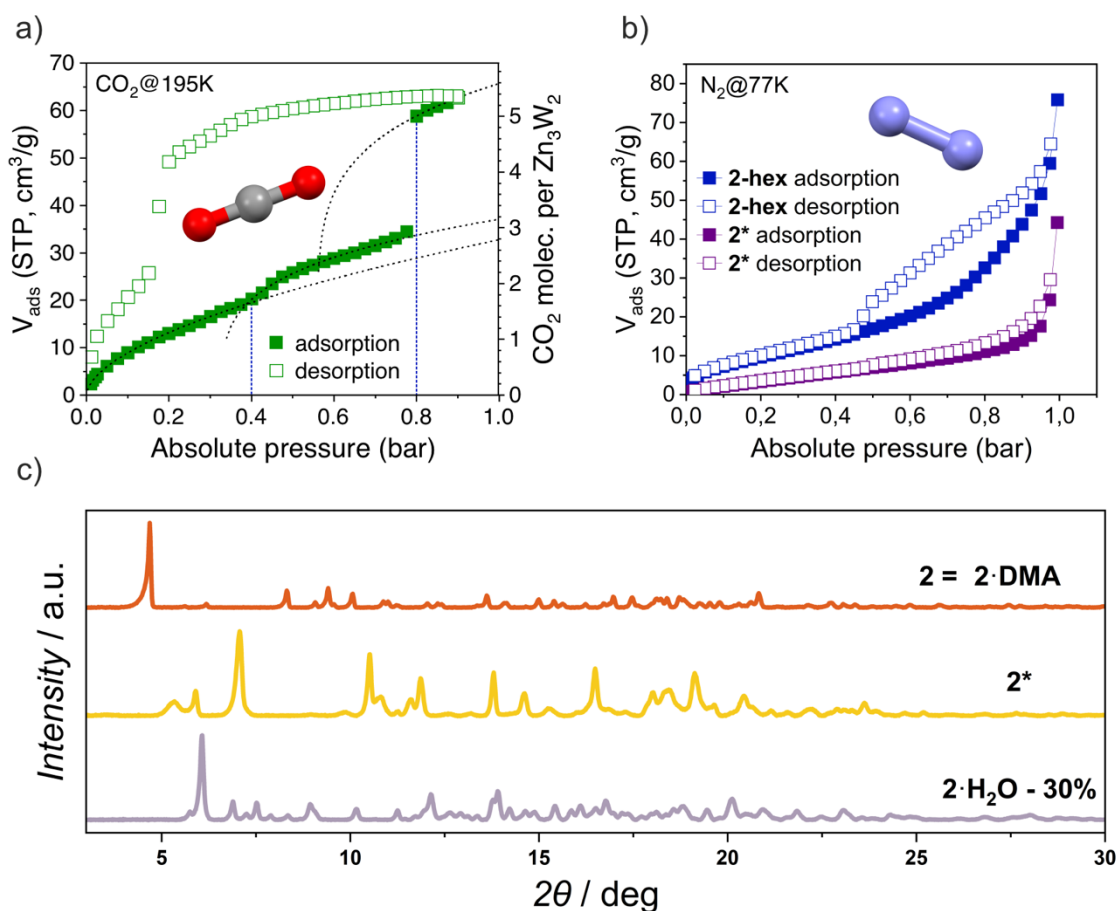
2.2.4. Low-pressure gas sorption

Figure S10. (a) CO_2 physisorption isotherms (195 K) with three Freundlich isotherms fitted (black dashed lines) and pressures of phase transitions marked (blue dashed lines). (b) N_2 physisorption isotherms (77 K) after two representative methods of activation (degassing): after simple heating under vacuum (**2***) and after pretreatment (multiple times) with hexane (**2-hex**), as low-surface-tension liquid, to preserve structure framework shape. (c) Room temperature powder X-ray diffraction (RT-PXRD) diffractogram acquired for polycrystalline **2** samples: as synthesized identically to nitrogen-dried (**2** and **2·DMA**, brick) after activation (**2*,** yellow), and for **2·H₂O** sample at RH=30% (gray).

A modified Freundlich equation was used to correctly match isotherms for different degrees of framework opening:

$$V = K \cdot (p - a)^{1/n}$$

where V means adsorbate volume (at STP, cm³/g), p means adsorbate partial pressure (bar), and K, a, n are parameters. The modification involves introducing a shift of the zeropoint to higher

pressures a. The parameters, pressure ranges of fitting, and correlation coefficient (R^2) are presented in Table S5.

Table S5. Parameters of Freundlich isotherms fitted to carbon dioxide adsorption isotherm (Figure S10a).

	Isotherm I	Isotherm II	Isotherm III
Pressure range (bar)	0.01-0.375	0.425-0.750	0.800-0.900
a (bar)	0.00	0.33	0.56
n	1.767	3.714	5.525
K (cm^3/g)	32.77	41.31	76.23
R^2	0.9989	0.9944	0.9969

Various methods of degassing prior to nitrogen sorption measurement were verified. Activation at room temperature, 50 and 100°C was tested. The use of methanol, DCM, and hexane to exchange DMA guest molecules was performed. For all of them, except the use of hexane, the shape of the isotherm was identical to the isotherm presented on Figure S10b (purple). Only hexane pretreatment supported very slight framework skeleton preservation. Therefore, for comparison purposes (Figure S10), purple (**2***) nitrogen isotherm was used.
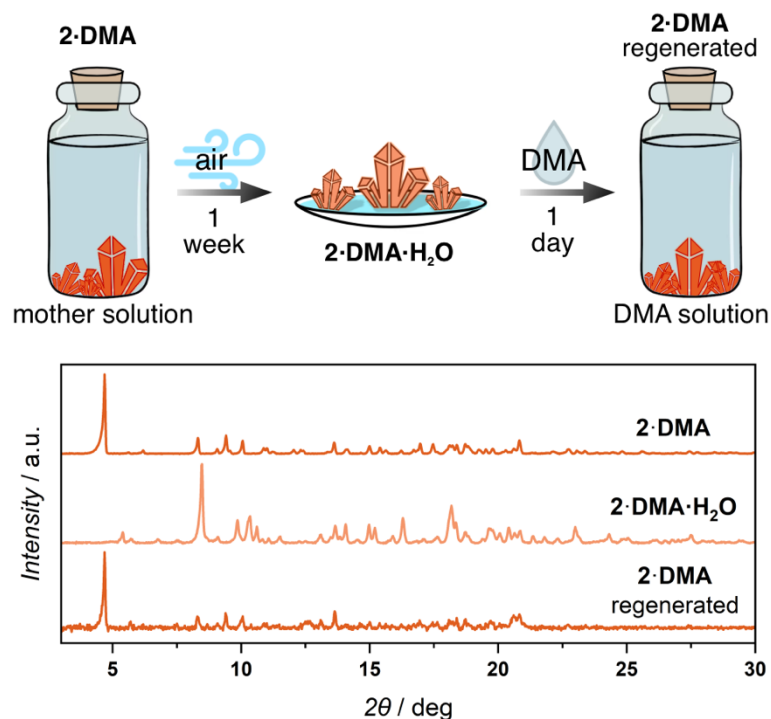
3. Regeneration processes

Figure S11. Scheme regeneration process (top) with experimental PXRD patterns of polycrystalline **2·DMA** samples.
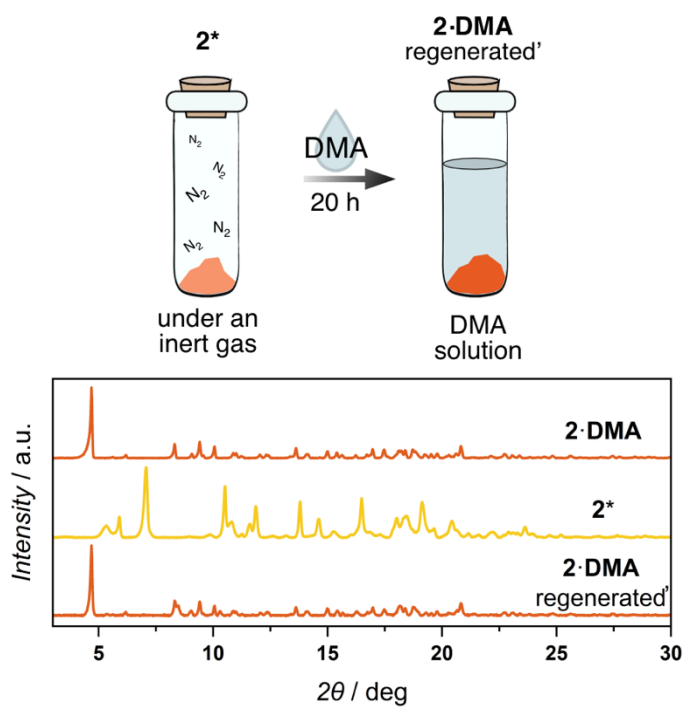

Figure S12. Scheme regeneration process (top) with experimental PXRD patterns of polycrystalline **2*** to **2·DMA** samples.
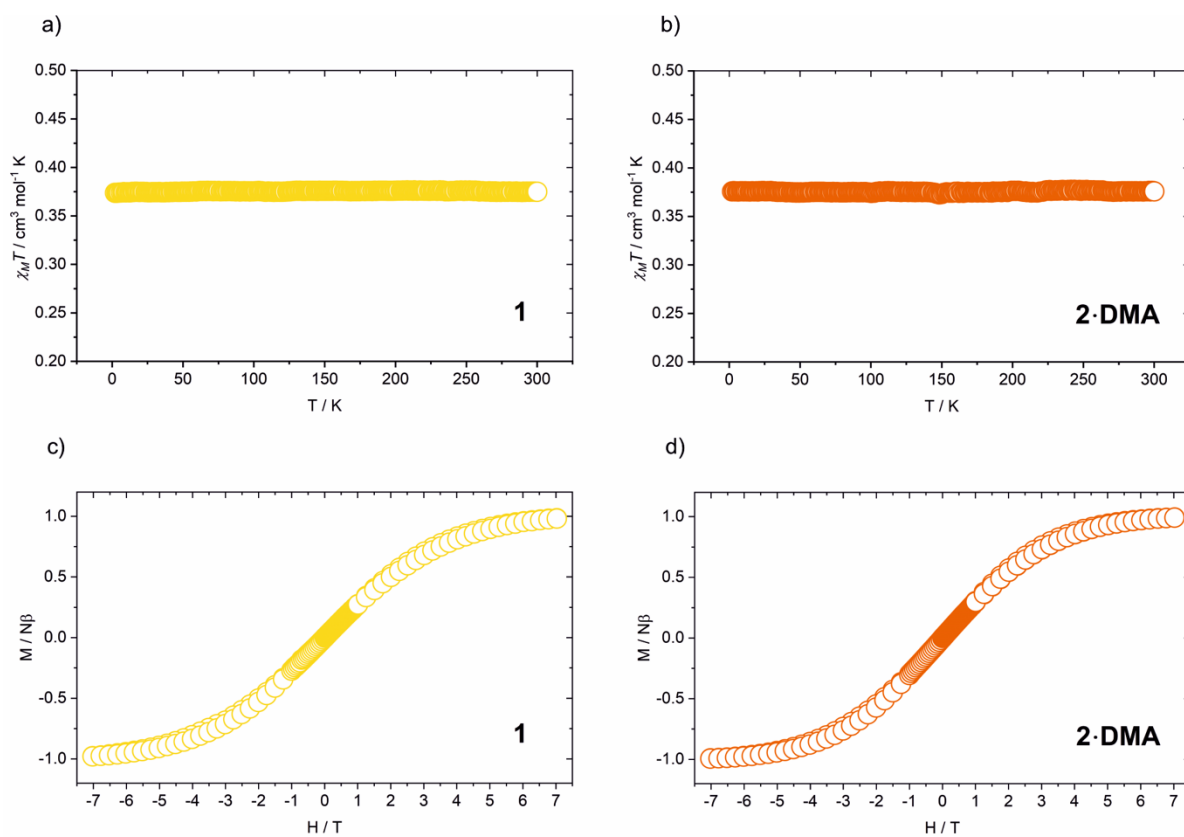
4. Magnetic characteristics

Figure S13. $\chi_M T(T)$ plot of **1** (a), **2·DMA** (b); M versus H plot at 2.0 K for **1** (c), **2·DMA** (d).
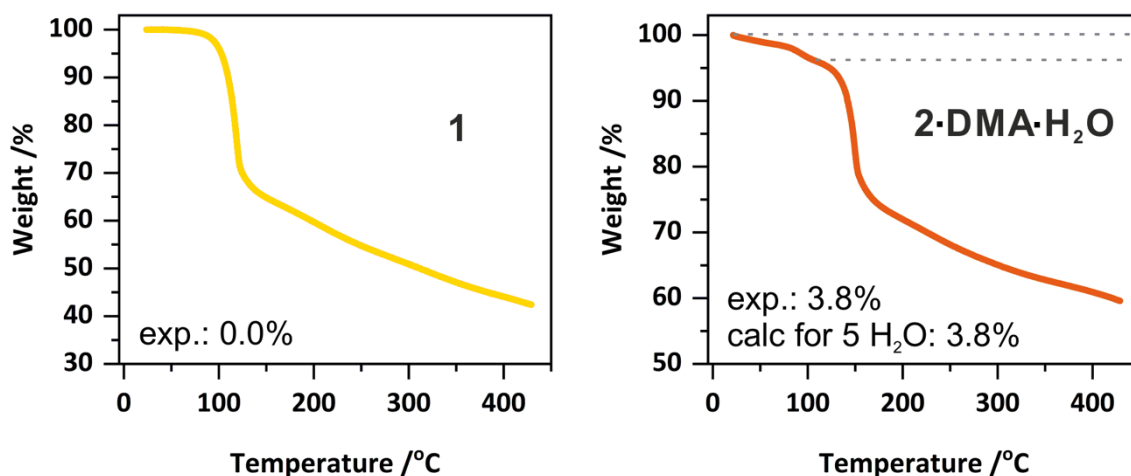
5. Thermogravimetric analysis

Figure S14. The thermogravimetric curves for both **1** and **2·DMA·H₂O** were obtained in the nitrogen atmosphere, at heating rate of 10 K per minute. Sample **1** remains stable up to $T = 100$ °C under a nitrogen atmosphere, after which a serious mass decomposition occurs. This includes the loss of crystallization DMA and, further, the decomposition of the cyanido-bridged skeleton. In contrast, sample **2·DMA·H₂O** exhibits moderate mass loss of ca. 3.8% in the RT – 150 °C range, reasonably attributable to five crystallization H_2O molecules per Zn_3W_2 formula unit, expected to be removed from the crystal first. This weight loss correlates with the number of solvent molecules, four DMA, and five H_2O determined by CHN analyses for the air-dried sample (*see* synthetic procedures in the Supplementary Information). This observation conforms to the tendency of **2·DMA·H₂O** to replace the native DMA solvent with the external H_2O solvent observed in DVS conditions, however, during drying in air the process seems to be less intense. Above $T = 150$ °C, desolvated **2·DMA·H₂O** undergoes further mass decomposition.

6. Details of materials and methods

Materials and syntheses

Materials

PPh$_4$Cl, PPh$_4$Br, Na$_2$WO$_4$, Zn(ClO$_4$)$_2$·6H$_2$O, 1,4,5,8-naphthalenetetracarboxylic dianhydride, 4-aminopyridine, and solvents (dimethylformamide, *N,N*-dimethylacetamide) were purchased from a commercial source (Sigma-Aldrich, Alfa Aesar, etc.) and used without further purification.

K$_4$[W^{IV}(CN)$_8$]·2H$_2$O,[4] was prepared according to the previously established synthetic procedures. (PPh$_4$)$_3$[W^V(CN)$_8$]·3H$_2$O organic salt was prepared through a metathesis reaction of potassium salt with chlorides or bromides of organic cations in distilled water.

Synthetic procedures for N,N'-di-(4-pyridyl)-1,4,5,8-naphthalenetetracarboxydiimide (4DPNDI)

N,N'-di-(4-pyridyl)-1,4,5,8-naphthalenetetracarboxydiimide (4DPNDI) was produced using a modified method described in literature.[5] To a stirred solution of 1,4,5,8-naphthalenetetracarboxylic dianhydride (2.5 g, 9.32 mmol) in degassed DMF (25 ml) under a flowing N$_2$ atmosphere, 4-aminopyridine (2.0 g, 21.3 mmol) was added. The mixture was then heated at 150 °C for 48 hours with continuous stirring under N$_2$. After cooling to room temperature, the resulting red-brown precipitate was filtered to yield a solid product. This solid was dissolved in 40 mL of DMF and subjected to recrystallization, which was repeated twice to obtain beige crystals. The final product was isolated via vacuum filtration, washed with cold DMF until the washings were colorless, and then dried. Yield: 3.00 g, 76.6%.

Synthetic Procedure for 1

A solution was prepared by mixing *N,N*-dimethylacetamide (DMA) with (PPh$_4$)$_3$[W^V(CN)$_8$]·3H$_2$O (0.35 g, 0.24 mmol in 30 mL of DMA), and Zn(ClO$_4$)$_2$·6H$_2$O (0.2 g, 0.54 mmol in 30 mL of DMA). This resulted in an immediately intense yellow solution, which was then sealed tightly in the vessel. Overnight, yellow crystals suitable for crystallographic measurements formed in the solution. Yield: 85.0%. The crystal structure was determined through single-crystal X-ray diffraction experiments. Freshly crystallized samples were examined using powder X-ray diffraction (PXRD) (Figure S1). Other techniques: FTIR spectroscopy (ATR, cm^{-1}): 2938 *v*(C-H), 2214, 2198, 2186, 2155 *v*(C≡N); ([W(CN)$_8$]$^{3-}$), other

peaks: 1606, 1512, 1419, 1403, 1262, 1189, 1109, 1010, and 966 (vibrations of PPh_4^+), and 607 (Figure S3); thermogravimetric analysis (Figure S14); elemental analysis: Calc. for $Zn_3W_2C_{48}H_{76}N_{24}O_{10}$ (M_w = 1713.18 g·mol^{-1}): C, 33.65%; H, 4.47%; N, 19.62%. Found: C, 33.5%; H, 4.5%; N, 19.4%. This composition is generally in agreement with the formula $\{Zn^{II}_3[W^V(CN)_8]_2(DMA)_8\}$ derived from SC XRD analysis but suggest a possible uptake of two additional H_2O molecules from the atmosphere in the course of time. The composition remains stable up to approximately 100°C, while above this temperature significant decomposition occurs with *ca.* 35% mass loss.

Synthetic Procedure for 2·DMA

N,N-dimethylacetamide (DMA) solutions of 4DPNDI (0.1 g, 0.24 mmol in 20 mL of DMA), $(PPh_4)_3[W^V(CN)_8]$·3H$_2$O (0.35 g, 0.24 mmol in 10 mL of DMA), and $Zn(ClO_4)_2$·6H$_2$O (0.2 g, 0.54 mmol in 20 mL of DMA) were mixed to give an intense orange solution immediately. The solution was tightly closed in the vessel. The orange crystals suitable for crystallographic measurements were obtained overnight. Yield: 80.0%. The crystal structure was determined through single-crystal X-ray diffraction experiments. Freshly crystallized samples were examined using powder X-ray diffraction (PXRD) (Figure S1). Other techniques: FTIR spectroscopy (ATR, cm^{-1}): 2936 v(C-H), 2202, 2195, 2153 v(C≡N) ($[W(CN)_8]^{3-}$), other peaks: 1719, 1678, 1637, 1603, 1499, 1398, 1353, 1257, 1189, 1014 (vibrations of PPh_4^+), 772 and 639 (Figure S3); thermogravimetric analysis (Figure S14); and elemental analysis: Calc. for $Zn_3W_2C_{80}H_{112}N_{30}O_{19}$ (M_w = 2361.84 g·mol^{-1}): C, 40.68%; H, 4.78%; N, 17.79%. Found: C, 40.5%; H, 4.8%; N, 17.9%. This composition suggests the presence of four DMA and five H_2O molecules as the crystallization solvents $\{Zn^{II}_3(DMA)_6[W^V(CN)_8]_2(4DPNDI)·4DMA·5H_2O\}$ (denoted as **2·DMA·H$_2$O**), which indicates the replacement of four native crystallization DMA molecules with five atmospheric H_2O molecules during air-drying. The volume of the resultant crystallization solvent set decreases compared to **2·DMA**, which is in line with the possible decrease of the volume of porosity qualitatively suggested by the PXRD patterns for **2·DMA** and **2·DMA·H$_2$O** (Figure S11). Above 150 °C, significant decomposition occurs most probably involving the remaining solvent molecules and components of the coordination skeleton (e.g. CN$^-$ ligands).

X-ray diffraction analysis.

Single crystal X-ray diffraction (SC-XRD) data for compound **1** were collected using two different diffractometers. The first set of data was acquired using a Rigaku XtaLAB Synergy (Dualflex) diffractometer equipped with a HyPix detector and a monochromatic Cu Kα X-ray source (λ = 1.54184 Å). The second set was collected using a Bruker D8 Venture diffractometer equipped with a Photon III detector and utilizing Mo Kα (λ = 0.71073 Å) radiation produced by a sealed microfusion tube. While the data from both diffractometers were consistent, superior parameters were achieved with the Bruker D8 Venture diffractometer. In contrast, the SC-XRD experiments for **2·DMA** were performed using a Bruker D8 Quest Eco diffractometer (Mo Kα, λ = 0.71073 Å radiation source with a graphite monochromator). All measurements were performed at 100 K. Data reduction and cell parameter refinement were carried out using the CrysAlis Pro,[6] or Apex4 for **1**, and Apex3 software[7] for **2·DMA**, which included the SAINT and SADABS programs. The intensities of reflections for the sample absorption were corrected using the multiscan method. Structures were solved by the intrinsic phasing method and refined anisotropically with weighted full-matrix least-squares on F^2 using the SHELXT[8] program with the Olex2 graphic interface.[9] Some soft SHELXT restraints (DELU, SIMU, DEFIX, ISOR) had to be used to correct the geometry of the disordered parts and the thermal parameters of the corresponding atoms. Heavy atoms were refined with anisotropic displacement parameters, whereas hydrogen atoms were assigned at calculated positions with thermal displacement parameters fixed to a value of 20 % or 50 % higher than those of the corresponding carbon atoms. The electron densities corresponding to the disordered solvent molecules of DMA in the voids were flattened using Solvent Mask (Olex 2 implementation of SQUEEZE procedure).

All structural figures were prepared using the Mercury software.[10] The results of the data collection and refinement have been summarized in Table S1, and selected bond lengths and angles are presented in Tables S2 and S3 in the ESI. CCDC: **1** – 2361511, **2·DMA** – 2361512 contain the supplementary crystallographic data for all the compounds, respectively. These data can be obtained free of charge from the Cambridge Crystallographic Data Centre www.ccdc.cam.ac.uk.data_request/cif.

Physical techniques.

PXRD data for phase purity confirmation were obtained using a Bruker D8 Advance diffractometer (Cu Kα radiation) at room temperature for ground crystalline samples loaded into glass capillaries under mother liquor (0.7 mm in diameter).

Thermogravimetric (TGA) curves for the polycrystalline samples were performed using a NETZSCH TG 209 F1 Libra under a flow of nitrogen (20 mL min^{-1}) and a temperature scanning rate of 10 °C min^{-1} with aluminum pans serving as holders. Data were collected within the temperature range of 25-450 °C.

Infrared spectra were recorded using a Thermo Scientific Nicolet iS10 FT-IR spectrophotometer equipped with an iD7 diamond ATR attachment.

^{1}H NMR spectra were recorded on Jeol spectrometer operating at 400 MHz in CDCl$_3$ and DMSO-d$_6$.

Gravimetric dynamic vapour sorption measurements were performed using a Surface Measurement System DVS Resolution apparatus. The crystalline samples of **2·DMA** were placed on the balance pan directly after filtration from DMA and kept under flow of dry nitrogen until constant mass was achieved (dm/dt = 0.002 %/min.). The isotherms were measured at 25 °C in the constatnt flow of nitrogen with appropriate solvent vapour in the range of p/p$_0$ of 0-98 % (H$_2$O) or 0-90 % (organic solvents). In each step the sample mass was stabilized to dm/dt = 0.002 %/min.

Volumetric gas sorption isotherms were measured on a Quantachrome Autosorb iQ-C-XR-XR EPDM instrument. Before measurements, samples were degassed 50 °C for 12 h (optimization of the degassing time was made, and no further changes were noted for extended time and for pre-exchange with volatile solvents such as methanol or hexane). The sorption measurements were carried out at 77 K for N$_2$, 195 K for CO$_2$. Temperature control was provided by using a liquid N$_2$ bath (77 K), an acetone: dry ice bath (195 K).

The magnetic measurements were probed with MPMS XL SQUID magnetometer. The microcrystals of all samples were sealed in glass tubes with a small amount of mother solution under vacuum. The DC magnetic susceptibilities were measured in the 2.0 – 300 K temperature range with a 2 K/min heating rate. Measurements were carried out with a DC applied field of 0.4 T (4000 Oe). The isothermal magnetizations were collected at 2.0 K in H_{dc} = -7 – 7 T range. The magnetic data were corrected for the diamagnetic contribution of the used glass tubes, and the sample itself using empirical and Pascal's constants, respectively.[11]

Calculations.

Continuous Shape Measure analysis for the coordination spheres of Zn and W in **1** and **2·DMA** were performed using SHAPE software ver. 2.1.[12]

The Zeo++ software was used for the structural analysis of the prepared PCP model (**2·DMA** without guest molecules). The specific surface area (1253.53 m^2/g) and pore volume (41.0%) of the prepared PCP model were calculated using a spherical probe with a radius of 1.86 Å, corresponding to the kinetic radius of CO_2 molecule.[13]

The underlying framework topology was determined and described by using TOPOS Pro software.[14]

The lattice parameters of **2*** were determined based on the **2·DMA** model using Le Bail mode in Fox v.2022.1 software.[15] The starting parameters were modified slightly and were later optimized by the fitting procedure. During the fitting also 20 polynomial background as well as pseudo Voigt peak shape parameters were fitted and gave final Rp about 24%.

Data availability

Crystallographic data can be obtained via https://www.ccdc.cam.ac.uk/data_request/cif, by emailing data_request@ccdc.cam.ac.uk, or by contacting The Cambridge Crystallographic Data Centre, 12 Union Road, Cambridge CB2 1EZ, UK; fax: +44 1223 336033.

7. Author Contributions

K.J.: investigation—syntheses, measurements and analysis of PXRD, TGA, IR spectroscopy; SC XRD structural measurement; crystal structure solution and refinement; description; data visualization; data curation; writing—original draft preparation, writing—review; J.K.: investigations—SC XRD structural measurement; crystal structure solution and refinement; magnetic measurements and interpretation of the data; writing—original draft preparation; T.M.M.: SC XRD structural measurement; crystal structure solution and refinement; writing—review; B.N.: DVS measurement and analysis; writing—original draft preparation, writing—review; D.J.: volumetric gas sorption measurement and analysis; IR spectroscopy measurements; writing—original draft preparation, writing—review; D.M.: volumetric gas sorption measurement and analysis; IR spectroscopy measurements; writing—original draft preparation, writing—review; B.G.: investigation—measurements and analysis of PXRD, data curation, writing—review; R.P.: funding acquisition; project administration; conceptualization; supervision; writing—original draft preparation; writing—review; corresponding author. All authors have read and agreed to the published version of the manuscript.

8. References to Supplementary Information

1 B. Nowicka, M. Rams, K. Stadnicka and B. Sieklucka, *Inorg. Chem.*, 2007, **46**, 8123–8125.

2 M. Heczko, E. Sumińska, B. Sieklucka and B. Nowicka, *CrystEngComm*, 2019, **21**, 5067–5075.

3 A. Pacanowska, M. Reczyński and B. Nowicka, *Crystals*, 2019, **9**, 45.

4 J. Szklarzewicz, D. Matoga and K. Lewiński, *Inorganica Chim. Acta*, 2007, **360**, 2002–2008.

5 S. Hernández, C. Ottone, S. Proto, K. Tolod, M. D. de los Bernardos, A. Solé-Daura, J. J. Carbó, C. Godard, S. Castillón, N. Russo, G. Saracco and C. Claver, *Green Chem.*, 2017, **19**, 2448–2462.

6 *E. CrysAlis Red and CrysAlis CCD*, Oxford Diffraction Ltd.:, Abingdon, UK., 2000.

7 *J. Neurosci. Methods*, 2008, **172**, 283–293.

8 G. M. Sheldrick, *Acta Crystallogr. A*, 2008, **64**, 112–122.

9 O. V. Dolomanov, L. J. Bourhis, R. J. Gildea, J. A. Howard and H. Puschmann, *J. Appl. Crystallogr.*, 2009, **42**, 339–341.

10 C. F. Macrae, I. Sovago, S. J. Cottrell, P. T. A. Galek, P. McCabe, E. Pidcock, M. Platings, G. P. Shields, J. S. Stevens, M. Towler and P. A. Wood, *J. Appl. Crystallogr.*, 2020, **53**, 226–235.

11 G. A. Bain and J. F. Berry, *J. Chem. Educ.*, 2008, **85**, 532.

12 D. Casanova, J. Cirera, M. Llunell, P. Alemany, D. Avnir and S. Alvarez, *J. Am. Chem. Soc.*, 2004, **126**, 1755–1763.

13 D. Ongari, P. G. Boyd, S. Barthel, M. Witman, M. Haranczyk and B. Smit, *Langmuir*, 2017, **33**, 14529–14538.

14 V. A. Blatov, A. P. Shevchenko and D. M. Proserpio, *Cryst. Growth Des.*, 2014, **14**, 3576–3586.

15 V. Favre-Nicolin and R. Černý, *J. Appl. Crystallogr.*, 2002, **35**, 734–743.